Journal of Power Sources 652 (2025) 237347

Contents lists available at ScienceDirect

Journal of Power Sources

journal homepage: www.elsevier.com/locate/jpowsour

Quantum-assisted machine learning screening for sustainable anode discovery in lithium-ion batteries

Marco Fronzi [a,b,*], Catherine Stampfl [b], Amanda Ellis [a], Eirini Goudeli [a,**]

[a] School of Chemical Engineering, University of Melbourne, Parkville VIC 3010, Australia
[b] School of Physics, University of Sydney, Camperdown, NSW 2006, Australia

HIGHLIGHTS

- Quantum-assisted machine learning screens 9835 crystal structures for LIB anodes.
- Identifies 211 thermodynamically stable materials with high lithium-ion mobility.
- Novel RE*(recyclable element)-based anodes support a sustainable circular economy.
- RE*-based materials outperform silicon anodes with enhanced stability and capacity.
- Combines DFT and ML for scalable, sustainable anode material discovery.

ARTICLE INFO

Keywords:
Lithium ion battery
Anode
Machine learning
Density functional theory

ABSTRACT

A comprehensive analysis of 9835 crystal structures, 211 of which are calculated to be thermodynamically stable, is presented, assessing their potential as anode materials for lithium-ion batteries. Density functional theory (DFT) calculations and advanced machine learning techniques are employed to explore the stability, lithium diffusion, bulk modulus and shear stress, along with the relationships between atomic orbital overlap, energy density, and ion mobility, which is a crucial factors for rapid charging capabilities. The study also examines the combined effects of elemental composition and crystallographic space groups to identify the key drivers of structural toughness. A number of crystal structures are identified as promising anode materials, with some standing out for their exceptional stability and efficient lithium-ion mobility. These materials demonstrate significant potential for high-capacity, durable battery anodes, highlighting the importance of a multidimensional approach in battery material development.

These insights provide a novel perspective on the interplay between physical, chemical, and electronic properties in optimising anode materials. This work offers valuable guidance for the future design and development of high-performance lithium-ion batteries, contributing to a more sustainable economy.

1. Introduction

The application of photovoltaics (PV) has been rapidly increasing over the past two decades, giving hope to a near-future transition to a renewable energy-based economy [1–3]. However, long-term sustainability will depend on the ability to recycle end-of-life panels, and the disposal of a very large quantity of obsolete photovoltaic modules predicted by 2050 represents both a significant environmental challenge and an opportunity for innovative recycling strategies [4–6].

Converting recycled PV materials into valuable battery components can support a circular economy where solar panel elements are reused to meet the demands of energy storage applications. Indeed, LIBs play a crucial role in sustainable energy systems, and their performance can be significantly improved by careful selection of anode materials with high energy capacity, mechanical stability, and robust cyclability. In this context, the key research question that drives this work is: "Can elements recovered from waste PV modules be integrated into new crystal structures that surpass or complement the capacity and durability of silicon-based anodes?" Recent research demonstrates the feasibility of recycling materials from waste panels for battery component fabrication [7–11].

The potential transformation of recycled photovoltaic (PV) materials into battery components not only facilitates resource conservation but also helps the solar industry minimise waste generation,

* Corresponding author at: School of Physics, University of Sydney, Camperdown, NSW 2006, Australia.
** Corresponding author.
E-mail addresses: marco.fronzi@sydney.edu.au (M. Fronzi), eirini.goudeli@unimelb.edu.au (E. Goudeli).

https://doi.org/10.1016/j.jpowsour.2025.237347
Received 19 September 2024; Received in revised form 29 April 2025; Accepted 9 May 2025
Available online 12 June 2025

particularly given that solar panel manufacturing in the semiconductor industry extensively uses elements such as nitrogen, fluorine, and boron, as well as transition metals like iron, nickel, cobalt, and manganese [10,12,13].

The prospect of recycling elements from decommissioned solar panels offers a opportunity to reduce material costs in the production of advanced anode materials, while promoting a circular economy. In addition to their availability, each selected element possesses distinctive electronic, chemical, and structural properties that could be strategically exploited to improve the performance of lithium-ion battery anodes. Nitrogen is capable of forming stable covalent bonds and modifying the electronic properties of carbon matrices, leading to enhanced electrical conductivity and electrochemical activity [14–16]. Boron, similar to nitrogen, can boost lithium storage capacity when introduced into carbonaceous frameworks through doping strategies [17]. Fluorine, due to its high electronegativity, facilitates the formation of highly stable fluorinated carbon materials, which can improve thermal stability and reduce voltage hysteresis, contributing to better cycling efficiency [18]. Iron, nickel, cobalt, and manganese, belonging to the transition metal group, exhibit variable oxidation states that enable reversible redox reactions essential for efficient energy storage [19]. Specifically, iron oxides, offer high theoretical capacities but face challenges related to conductivity and volume expansion during cycling [20]. Nickel, provides a balance between capacity and mechanical robustness [21]. Cobalt, known for its high thermal stability, can promote the cyclability and structural integrity of anodes, albeit with concerns regarding cost and toxicity [22]. Finally, manganese stands out due to its high structural stability and low volume expansion, particularly when incorporated into oxide-based frameworks [23].

Despite its promise, the transformation of recycled photovoltaic elements into commercially viable battery components faces major challenges, chiefly the need to overcome compositional variability and to integrate the materials into structures that ensure high capacity, mechanical stability, and long-term performance over repeated charge–discharge cycles.[24,25]

This paper aims to contribute to the ongoing research in lithium ion battery (LIB) technology by providing a quantum mechanical trained machine learning (ML) assisted screening of unexplored crystal structures chosen upon considerations of the economic system and a scientifically grounded rationale for the inclusion of these elements in anode design. The properties of each element, are dissected to understand their potential impact on the performance of LIB anodes, addressing challenges such as volume expansion, conductivity, and cost.

Here, we address the conversion of waste solar panels into commercially valuable battery materials through a systematic screening of thousands of potential crystal structures, followed by the identification of thermodynamically stable structures, and a targeted evaluation of their mechanical and electrochemical properties, compared to conventional silicon-based anodes. We focus our analysis on screening crystal materials that, incorporating recycled elements, can provide an alternative to conventional silicon-carbon composites, maintaining performances comparable performances [10,12]. We aim to: (1) apply quantum mechanical and machine learning (ML) models to identify how structural, electronic, and compositional factors affect energy density, lithium-ion mobility, and mechanical stability; and (2) understand whether incorporating elements such as C, O, N, B, F, Fe, Ni, Co, and Mn into Si-based anodes can deliver higher capacity and mechanical robustness compared to established silicon-based electrodes (Table 1 reports a brief indicative summary of selected elements indicating their properties and potential benefits of each element). Here, carbon and oxygen are additionally included due to the carbon proven improvement in phase stability, and to the unavoidable oxygen presence in the realistic working environment [26–28]. The core objective of this study is to identify novel anode materials for lithium-ion batteries. Specifically, this work contributes: (i) a high-throughput screening of thermodynamic stability and diffusion properties across 9835 candidate structures; (ii) the identification of high-potential anode materials combining structural integrity with optimal Li-ion transport; and (iii) the mapping of chemical and physical footprints indicative of stable and high-capacity material. In summary, while the scientific contribution of this work lies in the modelling approach and predictive insights, its practical relevance pertains to guiding the discovery of next-generation anode materials for lithium-ion batteries.

The quantum-assisted machine learning approach leverages accurate and precise data from density functional theory (DFT) calculations, capturing complex material behaviours at a fundamental level and enabling the prediction of material properties with high accuracy and efficiency [29,30]. By integrating quantum-derived datasets into machine learning models, this method transcends the limitations of traditional computational approaches and becomes a critical element in advancing material discovery and understanding complex behaviours that are not easily deducible from raw computational data alone.

2. Methodology

Ab-initio calculations based on periodic Density Functional Theory (DFT) are carried out to compute the electronic structure and derive key properties. We combine these data with machine learning approaches to predict mechanical properties and guide the selection of stable and high-capacity anode candidates.

We used a two-step approach:

1. We generated a dataset of 9835 crystal structures composed of Li, Si, C, O, N, B, F, Fe, Ni, Co, and Mn—elements commonly found in photovoltaic waste and known to influence the electrochemical and structural behaviour of lithium-based battery systems. The structures were obtained using automated high-throughput workflows built on the `pymatgen` and `ase` Python libraries. Structural prototypes were expanded into chemically substituted derivatives using enumeration algorithms such as `enumlib`, which systematically generate all symmetry-distinct configurations from a given parent lattice. Structures with redundant atomic arrangements or artificial distortions were excluded based on symmetry analysis and unit cell volume constraints. Only elemental combinations that allowed for formal oxidation states consistent with charge neutrality were retained; compositions requiring extreme or non-integral valences were excluded to ensure chemical plausibility. We select only crystals with unit cell volumes between 10 $Å^3$ and 2400 $Å^3$, corresponding to a typical atomic packing density range of 5–35 $Å^3$ per atom, to eliminate unrealistic geometries. Crystallographic symmetries were enforced by applying space group analysis and retaining only those structures belonging to the 230 well-defined space groups. Structures with symmetry-related degeneracies or redundant atomic arrangements were reduced to their primitive forms. Artificial distortions – such as unrealistically elongated bonds or asymmetric unit cells – were filtered by excluding any structure with bond lengths deviating by more than 20% from standard covalent radii or with unit cell angles deviating more than 10 ° from ideal values in high-symmetry systems.

Although the dataset does not aim to be exhaustive, it spans a broad range of crystallographic symmetries and stoichiometric ratios, reflecting a diverse and realistic sample of chemically and structurally viable compounds. A statistical overview of the final dataset is presented in Fig. 1, illustrating the distributions of space group numbers, unit cell volumes, and the number of unique elements per compound. These distributions highlight the structural and chemical diversity of the dataset, which is essential for developing generalisable machine learning models and performing robust high-throughput screening of potential anode materials.

Spin-polarised DFT calculations are carried out by employing the Vienna *Ab-initio* Simulation Package (VASP), to calculate Gibbs free energy, density of states and orbital overlapping [31–34]. The interactions between core and valence electrons were considered through

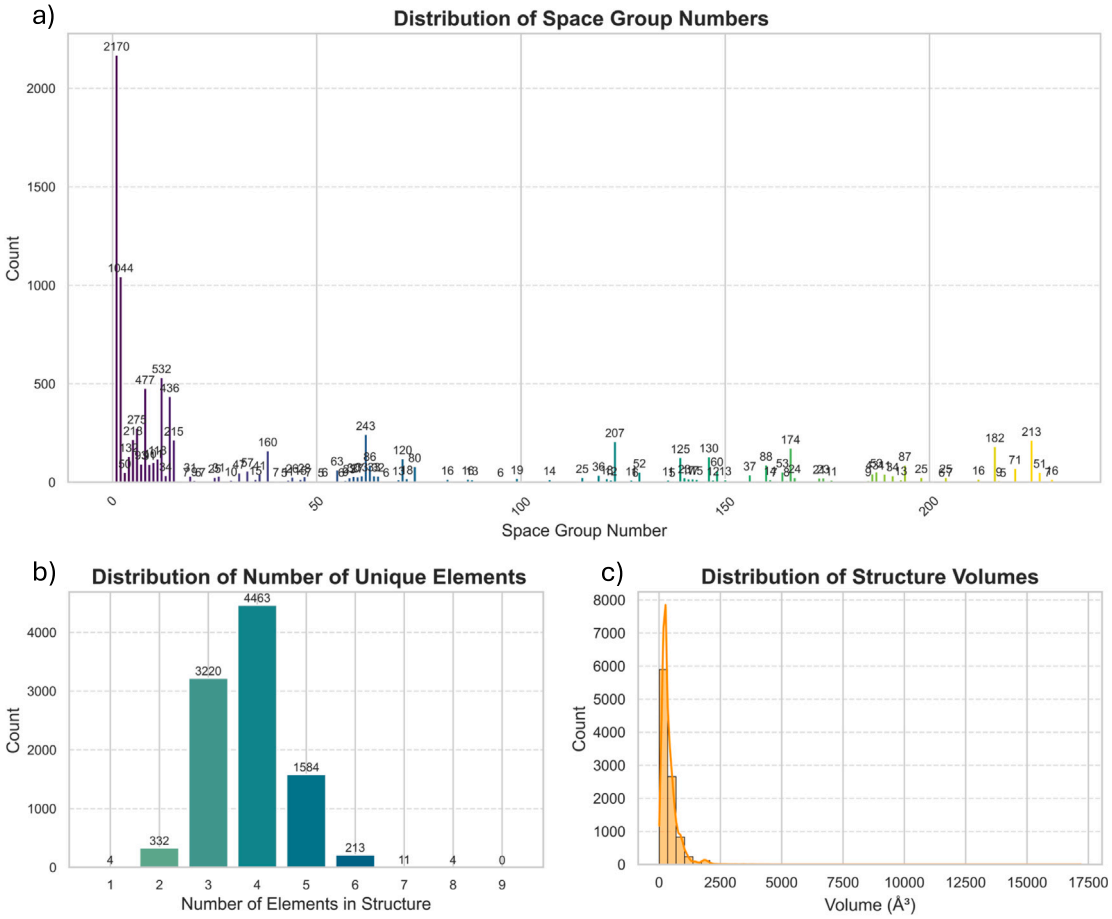

Fig. 1. Statistical characterisation of the dataset comprising 9835 Li-based crystal structures. (a) Distribution of crystallographic space group numbers, illustrating the prevalence of common symmetries. (b) Frequency of unique element counts per structure, indicating the compositional complexity across the dataset. (c) Histogram of unit cell volumes (in Å^3), showing the diversity in crystal size and density.

projector augmented-wave potentials, with valence electrons represented by periodic plane waves at a cut-off energy of 550 eV [35]. The pseudo-potentials of lithium were handled by integrating the s electrons into the valence electron configuration. The exchange–correlation functional was addressed within the Perdew, Burke, and Ernzerhof (PBE) formulation [36]. The k-point mesh was tailored individually due to the different cell sizes. We applied thermodynamic considerations to identify stable candidates, and only those that lay on the convex hull were considered stable, reducing the original set of 9835 to 211 stable structures. This thermodynamic assessment is crucial for filtering out the computationally feasible crystal structures ensuring that our focus is on the most promising candidates for practical implementation in device-scale or industrial applications.

The dataset of thermodynamically stable structures includes a diverse range of crystal compositions, with only a few more complex multi-element systems. The crystallographic space groups of these crystals includes both high-symmetry and low-symmetry groups and with a cell sizes ranging from around 2.5 Å to over 13 Å.

To investigate Li diffusion in the generated structures, *ab-initio* Molecular Dynamics simulations (AIMD) were conducted at 300 K using a Nosé-Hoover thermostat, with a time step of 2.0 fs at the gamma point [37]. Each crystal cell was appropriately expanded to ensure negligible interactions between the diffusing Li atom and its replica under periodic boundary conditions. The Li-ion diffusion coefficient D_{coeff} was calculated from the velocity autocorrelation function: [38]

$$D_{coeff} \approx \sum_{i=1}^{N-1} \frac{C_v(t_i) + C_v(t_{i+1})}{2} \Delta t \tag{1}$$

where $C_v(t_i)$ is:

$$C_v(t) = \langle \mathbf{v}(t) \cdot \mathbf{v}(t+\tau) \rangle \quad . \tag{2}$$

2. DFT calculations were used to generate machine learning models. Random Forest (RF) and eXtreme Gradient Boosting (XGBoost) were chosen due to their efficacy for handle high-dimensional, nonlinear data, and strong performance in regression tasks relevant to materials informatics (bulk modulus, shear stress, diffusion coefficients) [39–42]. These ensemble-based models have been extensively validated for predicting battery-related properties such as lithium diffusion, bulk modulus, and theoretical capacity [41,43]. In addition, RF provide measures of feature importance, enabling interpretability and identification of key structural descriptors that influence capacity.

To train predictive models for bulk modulus and shear stress, we included a comprehensive set of structure and composition-based descriptors derived primarily from the Materials Agnostic Platform for Informatics and Exploration `Magpie` feature library [39]. These features capture elemental, structural, and electronic characteristics of the anode materials and were chosen for their interpretability and established relevance in materials informatics. A total of 253 numerical features were initially extracted, and feature selection using LASSO regression was performed to identify the most relevant descriptors, ultimately retaining 71 features with non-zero coefficients to reduce model complexity while maintaining predictive accuracy [44].

In the ML training, we included metastable crystals randomly selected within different clusters generated using KMeans models. The large training set can offer a diverse example of electronic structure, as well as functional and structural descriptors, that may correlate with

Table 1
Characteristics of selected elements considered for alternative anode materials for lithium-ion batteries. The table summarises the unique properties and potential benefits of each element as suggested by data in the literature.

Element	Properties	Ref.
Nitrogen	Enhances conductivity and electrochemical activity	[15]
Boron	Amplify Li-ion storage capacity	[17]
Fluorine	Reduces voltage hysteresis and offers thermal stability	[18]
Iron	Increases capacity (although challenges in volume expansion)	[20]
Nickel	Increases capacity and stability in alloys/oxides	[21]
Cobalt	Improves thermal stability, limited by cost and toxicity	[22]
Manganese	Abundant and environmentally friendly	[23]

anode capacitance. While these phases may not be thermodynamically stable under standard operating conditions, their presence expands the diversity of the dataset, thereby enhancing the statistical robustness and the overall significance of the resulting analysis.

Random Forest (RF) and eXtreme Gradient Boosting (XGBoost) model were implemented and employed as an ensemble learning technique regression tasks to calculate bulk modulus and shear stress. These models ensures robustness in handling complex, non-linear relationships, as reported in the literature [42,44,45]. Random Forest (RF) models were used to assess the importance of a few features in predicting the volumetric capacity of anode materials, defined as the amount of electrical charge the anode can store per unit volume [46].

We employed 10-fold cross-validation strategy to measure the model's accuracy using two different metrics: the mean squared error (MSE) and the coefficient of determination (R^2). By averaging the R^2 and MSE scores across all folds, we derived robust estimates of the model's predictive performance. This rigorous validation framework ensured that the reported metrics reliably reflect the Random Forest model's generalisability and stability when predicting on unseen data. For model interpretability, SHapley Additive exPlanation (SHAP) values were employed to quantify the contribution of each feature to the model's predictions. SHAP attributes to selected (i.e. DFT calculated) features a fair and consistent importance value, gaininig intuitive insights into variablesinfluence into model's predictions, highlighting the key factors in the model predictions and providing a comprehensive overview of the interplay between various factors [46,47].

3. Results and discussion

In this section, results are presented from a comprehensive analysis focusing on the maximum theoretical capacity of various crystal structures, in order to identify crystal structures that potentially outperform traditional silicon anodes. This analysis incorporates structural, functional, and thermodynamic properties, such as Gibbs free energy, Li diffusion, and elasticity, as detailed in Tables 2 and 3. The investigation involves two performance indicators. Firstly, the maximum theoretical capacity (MTC), reflecting the energy storage capability of the materials, was calculated based on the number of electrons extractable upon delithiation of each crystal. This metric, referred to as Li maximum theoretical capacity, is detailed in the referenced literature [48]. Additionally, the full capacity of the crystals was computed by considering the total number of electrons available, providing a benchmark to assess how closely the Li maximum theoretical capacity approaches the maximum possible capacity. Li MTCs, involving the estimation of the net charge upon complete delithiation, are reported for the top 40 performing crystals in Table 2. Secondly, as indicators of anodic mechanical and electrochemical performance, Gibbs free energy, bulk modulus, shear stress, and Li diffusion were evaluated and presented in Table 3, assessing the structural integrity and resilience of the materials under operational conditions and cycling. The selection of these specific mechanical properties aligns with their relevance in determining the durability and reliability of anode materials in real-world battery applications. The maximum theoretical capacities (MTC) of selected crystals have been normalised against the standard benchmark of silicon of 4200 mAg^{-1}. This benchmarking provides contextual comparison with established LIB anode materials, such as different carbon phases including petroleum coke or graphite, demonstrating capacities ranging from 372 mAg^{-1} to 4200 mAg^{-1} [49–51]. Among the analysed compounds, $Li_{47}Ni_8O_{32}$ shows the highest theoretical capacity, measured at 2.24 (see Table 2), exceeding the capacity of silicon by more than double outperforming current industry standards. The same elemental combination can also yield other high-capacity phases, such as $Li_{23}Ni_{17}O_{40}$ and $Li_{19}Ni_{23}O_{42}$, indicating the compositional versatility and structural tunability intrinsic to these crystal systems. The literature confirms how several $Li_xNi_yO_z$ stoichiometries can be synthesised to achieve stable, high-capacity lithium storage performance, suggesting the significant elemental synergy and potential for long-term stable and high-capacity lithium storage systems [52–54]. Other notable compounds shown in Table 2, such as lithium-iron and lithium-cobalt oxides ($Li_{35}Fe_8O_{32}$ and $Li_{21}Co_8O_{18}$), have calculated capacities greater than 1.0, which represents a considerable enhancement over traditional materials. Previous DFT calculations have demonstrated that in $LiCoO_2$, oxygen anions actively participate in charge compensation during delithiation, contributing to the material's electrochemical capacity through anionic redox reactions; similarly, in lithium-rich layered oxides containing iron, DFT studies reveal that oxygen redox processes occur alongside transition metal redox, collectively enhancing the overall capacity of these materials [55,56]. The role of oxygen in these compounds may be particularly significant, potentially aiding in boosting electrochemical capacity through redox reactions and several Li-O stoichiometries incorporating Fe and Co have been identified as promising LIBs anode material [57–60]. However, one of the limitation of tested anodes, is the strong dependence on the cathode half potential, which may limit their application. Nevertheless, although this class of anode materials may not be appropriate candidates for the conventional LIBs, but they are still good choices for new types of electrochemical energy storage systems such as hybrid battery/super-capacitor.[61]

The inclusion of nitrogen, as seen in $Li_{19}Mn_5N_9$ and $Li_{36}Fe_{10}N_{24}$, suggests alterations in the electronic structure, which could improve the conductivity and stability of the anode materials, as also suggested by Cheng-Che et al. and Ma et al. [62,63] Similarly, theoretical analyses of Li_7MnN_4 using Density Functional Theory (DFT) within the Generalized Gradient Approximation (GGA) validate the electrochemical activity and structural integrity of lithium manganese nitrides, supporting our findings; moreover, Fe-rich nitrides have demonstrated reversible lithium cycling with moderate voltage hysteresis, complementing our results [64,65].

The distribution of largest capacities is reported in Fig. 2. Here, the majority of high capacity structures (indicated by the red dotted) have MTC exceeding 0.75, with several having capacities approaching that of silicon. This highlights the potential of these materials as competitive alternatives to current anode performance standards. A recurring theme in these findings is the ability of these multi-elemental compositions to meet or exceed the capacities of conventional silicon anodes, paving the way for the next generation of high-capacity, sustainable lithium-ion batteries.

The Gibbs free energies and diffusion coefficients for various crystal structures were determined using DFT and AIMD, respectively. In addition, the bulk modulus and shear stress of these structures were computed with machine learning Random Forest models, achieving a maximum accuracy levels of $R^2 \geq 0.97$ (details can be found in the SI). Orbital overlap calculations were conducted by integrating the overlapping projected Density of States (pDOS) in the energy range of −5 eV to 0 eV, with the reference point set at 0 eV, corresponding to the Fermi Energy. Table 3 provides a detailed view of these properties for a selection of crystal structures, chosen for their thermodynamic stability. These structures display promising characteristics for anode applications in lithium-ion batteries. A critical factor in determining battery

Table 2
Maximum theoretical capacity (MTC) of the 40 best performing crystals out of 9835 possible crystals. The capacity has been normalised with respect to that of Si (4200 mAg^{-1}).

Formula	Reaction	MTC
$Li_{47}Ni_8O_{32}$	$Li_{47}Ni_8O_{32} \rightarrow Ni_8O_{32}+47Li^++47e^-$	2.24
$Li_{35}Fe_8O_{32}$	$Li_{35}Fe_8O_{32} \rightarrow Fe_8O_{32}+35Li^++35e^-$	1.67
$Li_{23}Ni_{17}O_{40}$	$Li_{23}Ni_{17}O_{40} \rightarrow Ni_{17}O_{40}+23Li^++23e^-$	1.10
$Li_{88}Si_{20}$	$Li_{88}Si_{20} \rightarrow Si_{20}+88Li^++88e^-$	1.05
$Li_{21}Fe_4O_{16}$	$Li_{21}Fe_4O_{16} \rightarrow Fe_4O_{16}+21Li^++21e^-$	1.00
$Li_{21}Co_8O_{18}$	$Li_{21}Co_8O_{18} \rightarrow Co_8O_{18}+21Li^++21e^-$	1.00
$Li_{42}Co_8O_{32}$	$Li_{42}Co_8O_{32} \rightarrow Co_8O_{32}+42Li^++42e^-$	1.00
$Li_{84}Si_{20}$	$Li_{84}Si_{20} \rightarrow Si_{20}+84Li^++84e^-$	1.00
$Li_{20}Co_{21}O_{40}$	$Li_{20}Co_{21}O_{40} \rightarrow Co_{21}O_{40}+20Li^++20e^-$	0.95
$Li_{20}B_{54}O_1$	$Li_{20}B_{54}O_1 \rightarrow B_{54}O_1+20Li^++20e^-$	0.95
$Li_{19}Co_4O_{16}$	$Li_{19}Co_4O_{16} \rightarrow Co_4O_{16}+19Li^++19e^-$	0.91
$Li_{19}Mn_5N_9$	$Li_{19}Mn_5N_9 \rightarrow Mn_5N_9+19Li^++19e^-$	0.91
$Li_{19}Ni_{23}O_{42}$	$Li_{19}Ni_{23}O_{42} \rightarrow Ni_{23}O_{42}+19Li^++19e^-$	0.91
$Li_{36}Fe_{10}N_{24}$	$Li_{36}Fe_{10}N_{24} \rightarrow Fe_{10}N_{24}+36Li^++36e^-$	0.86
$Li_{17}Co_4O_{16}$	$Li_{17}Co_4O_{16} \rightarrow Co_4O_{16}+17Li^++17e^-$	0.81
$Li_{17}Ni_{11}O_{28}$	$Li_{17}Ni_{11}O_{28} \rightarrow Ni_{11}O_{28}+17Li^++17e^-$	0.81
$Li_{34}Co_6O_{24}$	$Li_{34}Co_6O_{24} \rightarrow Co_6O_{24}+34Li^++34e^-$	0.81
$Li_{17}Fe_6Si_{12}O_{42}$	$Li_{17}Fe_6Si_{12}O_{42} \rightarrow Fe_6Si_{12}O_{42}+17Li^++17e^-$	0.81
$Li_{17}Fe_4C_{16}O_{48}$	$Li_{17}Fe_4C_{16}O_{48} \rightarrow Fe_4C_{16}O_{48}+17Li^++17e^-$	0.81
$Li_{16}Fe_4Si_1O_{16}$	$Li_{16}Fe_4Si_1O_{16} \rightarrow Fe_4Si_1O+16Li^++16e^-$	0.76
$Li_{32}Co_6O_{24}$	$Li_{32}Co_6O_{24} \rightarrow Co_6O_{24}+32Li^++32e^-$	0.76
$Li_{15}Mn_2O_{12}$	$Li_{15}Mn_2O_{12} \rightarrow Mn_2O_{12}+15Li^++15e^-$	0.72
$Li_{15}Fe_2O_{12}$	$Li_{15}Fe_2O_{12} \rightarrow Fe_2O_{12}+15Li^++15e^-$	0.72
$Li_{15}Ni_{14}O_{28}$	$Li_{15}Ni_{14}O_{28} \rightarrow Ni_{14}O_{28}+15Li^++15e^-$	0.72
$Li_{30}Si_8$	$Li_{30}Si_8 \rightarrow Si_8+30Li^++30e^-$	0.72
$Li_{15}Mn_{15}Si_1O_{32}$	$Li_{15}Mn_{15}Si_1O_{32} \rightarrow MnSi_1O_{32}+15Li^++15e^-$	0.72
$Li_{30}Fe_8O_{32}$	$Li_{30}Fe_8O_{32} \rightarrow Fe_8O_{32}+30Li^++30e^-$	0.72
$Li_{15}Mn_{21}O_{43}$	$Li_{15}Mn_{21}O_{43} \rightarrow Mn_{21}O_{43}+15Li^++15e^-$	0.72
$Li_{14}Co_{13}O_{28}$	$Li_{14}Co_{13}O_{28} \rightarrow Co_{13}O_{28}+14Li^++14e^-$	0.76
$Li_{28}Mn_4O_{18}$	$Li_{28}Mn_4O_{18} \rightarrow Mn_4O_{18}+28Li^++28e^-$	0.76
$Li_{28}Fe_8O_{26}$	$Li_{28}Fe_8O_{26} \rightarrow Fe_8O_{26}+28Li^++28e^-$	0.76
$Li_{28}Mn_{10}F_{48}$	$Li_{28}Mn_{10}F_{48} \rightarrow Mn_{10}F_{48}+28Li^++28e^-$	0.76
$Li_{13}Fe_2O_{12}$	$Li_{13}Fe_2O_{12} \rightarrow Fe_2O_{12}+13Li^++13e^-$	0.62
$Li_{13}Mn_2O_{12}$	$Li_{13}Mn_2O_{12} \rightarrow Mn_2O_{12}+13Li^++13e^-$	0.62
$Li_{13}Ni_9O_{22}$	$Li_{13}Ni_9O_{22} \rightarrow Ni_9O_{22}+13Li^++13e^-$	0.62
$Li_{13}Mn_8O_{24}$	$Li_{13}Mn_8O_{24} \rightarrow Mn_8O_{24}+13Li^++13e^-$	0.62
$Li_{26}Mn_4O_{18}$	$Li_{26}Mn_4O_{18} \rightarrow Mn_4O_{18}+26Li^++26e^-$	0.62
$Li_{13}Ni_{15}O_{28}$	$Li_{13}Ni_{15}O_{28} \rightarrow Ni_{15}O_{28}+13Li^++13e^-$	0.62
$Li_{13}Co_{15}O_{28}$	$Li_{13}Co_{15}O_{28} \rightarrow Co_{15}O_{28}+13Li^++13e^-$	0.62
$Li_{26}Si_8$	$Li_{26}Si_8 \rightarrow Si_8+26Li^++26e^-$	0.62

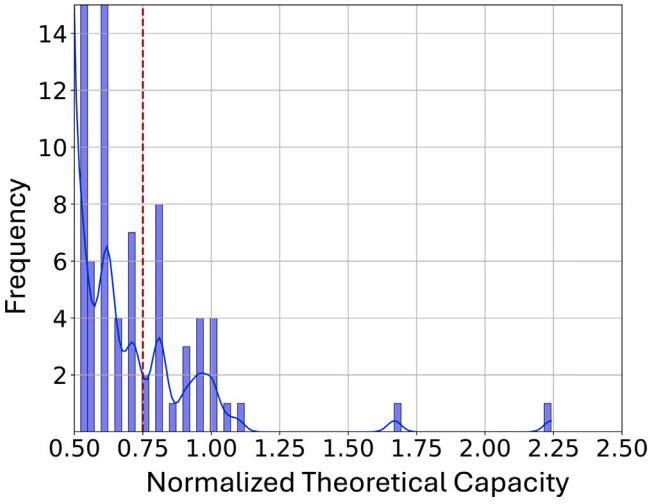

Fig. 2. Histogram of maximum theoretical capacity (MTC) greater than 0.5 when normalised with respect to that of Si per unit formula out of the among the 9835 structures considered.

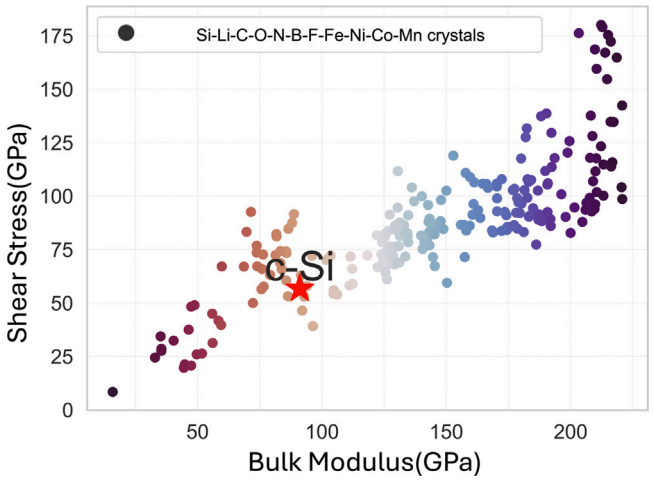

Fig. 3. Distribution of Bulk Modulus and Shear Stress (both in GPa) for the thermodynamically stable crystal structures. The colour gradient, ranging from dark brown to dark blue, represents increasing mechanical hardness—soft crystals appear brown, while hard crystals are shown in blue. The star marks the position of crystalline silicon (c-Si), serving as a reference point to illustrate the spread of micro-hardness among the analysed structures. (For interpretation of the references to colour in this figure legend, the reader is referred to the web version of this article.)

safety and lifespan is the Gibbs free energy at equilibrium. It was calculated that structures exhibiting high capacity also show lower Gibbs free energy values in comparison to crystalline silicon (c-Si). This pattern implies enhanced stability during battery operation, as lower Gibbs free energy typically aligns with better structural integrity and a lower likelihood of reactions that could deteriorate the battery over time. In-depth analysis of the data in Table 3 leads to conclusions regarding the performance of these materials and aids in identifying crystal structures with outstanding performance relative to conventional silicon anodes. For instance, $Li_{84}Si_{20}$ is distinguished by high thermodynamic stability, as indicated by favourable Gibbs free energy values in both neutral and charged states of −2.77 eV and −2.97 eV, respectively. Its MTC of 1, along with notable diffusion coefficients ($D^0_{coeff} = 3.10 \times 10^{-13}$ cm^2s^{-1} and D^+_{coeff}=3.90 × 10^{-12} cm^2s^{-1}), implies a potential edge in lithium-ion mobility over other structures. Furthermore, $Li_{16}Si_2O_{12}$ shows high lithium overlap, suggesting higher capacity for lithium incorporation within the crystal lattice, whereas the overall overlap values, indicative of the degree of electron interaction, point towards improved electrical conductivity for efficient battery operation [66]. Our analyses underscore the potential of $Li_{16}Si_2O_{12}$ and $Li_{24}Co_4O_{16}$ as promising lithium-ion conductors, attributed to their structural characteristics and electronic properties. Specifically, $Li_{24}Co_4O_{16}$ exhibits a layered architecture with pronounced Co–O covalency, a feature that has been correlated with enhanced electronic conductivity in $LiCoO_2$ and related systems [67]. Notably, $Li_{24}Co_4O_{16}$ is predicted to have a slightly elevated voltage plateau during the delithiation process, which may be attributed to the higher cobalt content influencing the material's electronic structure [67].

$Li_{84}Si_{20}$, having a calculated MTC of 1.00 and favourable Gibbs free energy values in both neutral and charged states, shows both high stability and lithium-ion mobility, with potential advantages over traditional anodes. Similarly, $Li_{56}Mn_8N_{32}$, containing nitrogen and manganese, shows notable mechanical strength, evident from high shear stress and bulk modulus values, suggesting improved durability and performance when synthesised as a single crystal, in line with Zhou et al. [64].

Structural insights

Shear stress (SS) and bulk modulus (BM) (see Fig. 3), representing the mechanical properties of anode materials, provide insights into

Table 3
Properties of selected lithium-based crystals to evaluate performance and stability in battery applications. The abbreviations are: MTC - Maximum Theoretical Capacity (normalised with respect to that of Si), SG - Space Group, $E_G(0)$ and $E_G(+)$ - Gibbs free energy in neutral and charged states (eV), D^0_{coeff} and D^+_{coeff} - Diffusion coefficients in neutral and charged states ($cm^2\ s^{-1}$), Li o.l. and Tot o.l. - Lithium and Total overlap (indicating electron interaction), SS (GPa) - Shear Stress (GPa), BM - Bulk Modulus (GPa).

formula	MTC	SG	$E_G(0)$	$E_G(+)$	D^0_{coeff}	D^+_{coeff}	Li o.l.	Tot o.l.	SS	BM
$Li_{84}Si_{20}$	1.00	216	−2.77	−2.97	3.10×10^{-13}	3.90×10^{-12}	2.28×10^{-4}	1.77	100	150
$Li_{30}Si_8$	0.71	220	−2.72	−2.73	2.30×10^{-13}	3.80×10^{-13}	2.49×10^{-4}	1.74	110	165
$Li_{26}Si_8$	0.62	55	−2.70	−2.67	1.50×10^{-11}	5.80×10^{-12}	2.79×10^{-4}	1.71	120	180
$Li_{16}Si_2O_{12}$	0.38	185	−5.99	−6.04	3.80×10^{-13}	2.70×10^{-12}	2.84×10^{-3}	3.32	130	195
$Li_{42}Si_{18}$	0.33	153	−3.34	−3.44	6.80×10^{-14}	3.10×10^{-12}	3.55×10^{-4}	1.62	140	210
$Li_{56}Mn_8N_{32}$	0.33	218	−5.59	−5.61	1.30×10^{-14}	2.10×10^{-14}	2.91×10^{-3}	9.53	150	225
$Li_{12}Fe_2N_8$	0.29	137	−5.75	−5.83	2.50×10^{-13}	4.10×10^{-12}	3.13×10^{-3}	11.17	160	240
$Li_{24}B_{16}O_{36}$	0.29	14	−7.35	−7.55	4.00×10^{-12}	1.20×10^{-12}	3.66×10^{-3}	8.56	170	255
$Li_{24}Co_4O_{16}$	0.29	137	−5.34	−5.47	1.70×10^{-13}	2.50×10^{-11}	3.37×10^{-3}	4.16	180	270
$Li_{24}Mn_4O_{16}$	0.29	137	−5.63	−5.60	1.40×10^{-12}	4.30×10^{-13}	3.19×10^{-3}	3.85	190	285
$Li_5Ni_3N_3$	0.24	189	−5.00	−5.04	1.80×10^{-12}	8.50×10^{-12}	5.41×10^{-3}	7.33	200	300
$Li_{80}Si_{16}N_{48}$	0.24	1	−4.31	−4.51	6.20×10^{-14}	1.20×10^{-13}	2.42×10^{-3}	9.95	210	315

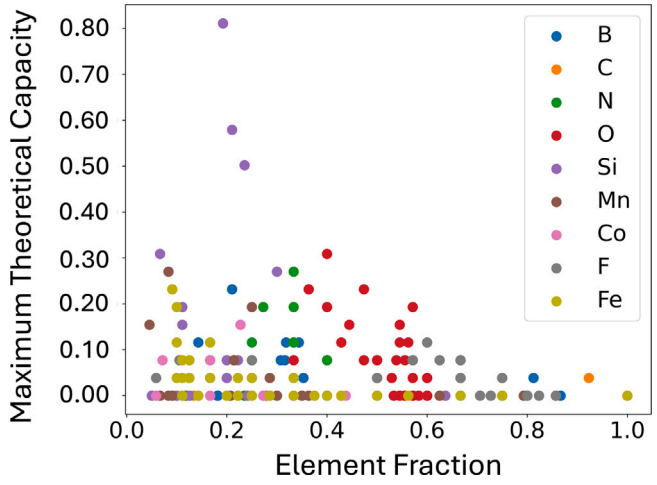

Fig. 4. Element fraction versus normalised maximum theoretical capacity for selected elements. The figure highlights the variability in MTC among different elemental compositions.

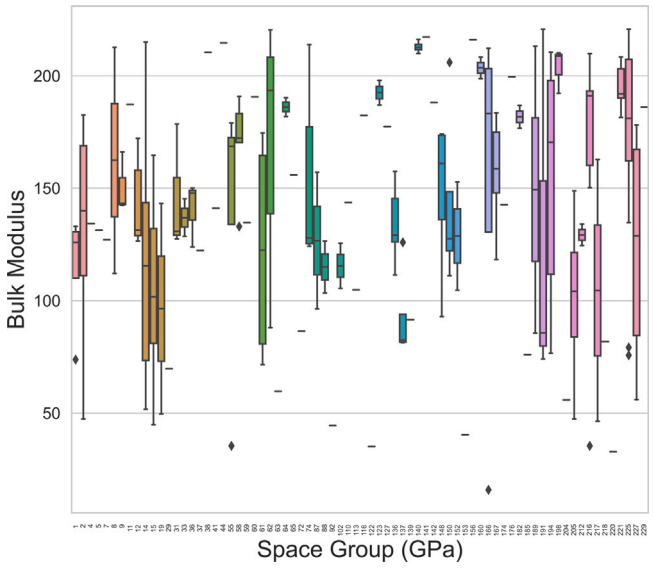

Fig. 5. Distribution of bulk modulus values across different space groups. Each box in the plot represents the distribution for a specific space group, with the interquartile range (IQR) from the 25th to the 75th percentile, the median value (horizontal line), and outliers plotted as dots. The colour scheme facilitates the identification of different lines.

their brittleness, hardness, and ductility. An analysis of micro-hardness across the 211 crystal structures, based on the methodology defined in previous work [68], reveals a linear distribution between shear stress and bulk modulus, with crystalline silicon (c-Si) located at approximately one-third of this distribution. Microhardness affects the material's resistance to volume changes during lithiation/delithiation cycles, which are a common cause of capacity fading in anodes. In a polycrystalline phase, where micro-hardness correlates with fragility, crystals with a large bulk modulus can negatively impact the structural properties of the anode [68]. Therefore, only a small portion of the entire set, approximately one-third, will improve structural properties anode. Among the stable structures, $Li_{56}Mn_8N_{32}$ has been identified to have robust mechanical properties when crystallised in a single phase, as evidenced by its high shear stress and bulk modulus, measured at 150 GPa and 225 GPa, respectively. These values suggest that a single phase of such materials could offer high mechanical stability in comparison to cubic silicon (c-Si), with shear stress and bulk modulus in the range of 54 GPa and 82 GPa [69]. On the other hand, when secondary phases are present, hardness might negatively influence the mechanical stability of a material, as micro-hardness can contribute to brittleness [25]. The inclusion of Mn has been associated with a reduction in micro-hardness and improved ductility in several manganese nitride systems, as reported by DFT studies, which aligns with the mechanical robustness observed here for Li–Mn–N compounds [70].

Elemental composition

The comparative analysis of the MTC, normalised with respect to silicon, for various elements, as depicted in Fig. 4, shows interesting trends. On average, elements such as Mn, Co, F, and Fe display a wide range of capacities, indicating the influence of their distinct electronic and structural features within the electrochemical environment. Transition metals like Mn and Co show notably variable capacity trends, which can be attributed to their ability to adopt multiple oxidation states, thereby facilitating enhanced electron transfer during lithiation and delithiation processes [71].

In contrast, the behaviour of elements such as F and Fe presents an opposite pattern. While Fe-containing compounds reach their highest capacities at relatively low elemental fractions, F-containing compounds attain their maximum (although relatively modest) capacities at higher fractions. This observation suggests a complex interplay between electronic structure, bonding environment, and Li-ion mobility within the crystal matrices, which impacts the electrochemical activity differently for each element.

A general evaluation of the top 40 highest-performing crystals, highlights that specific elements consistently contribute to higher capacities. In particular, nickel Ni, Fe and Co emerge as the dominant contributors, reinforcing the essential role of transition metal chemistry – particularly the capacity to access multiple oxidation states – in dictating lithium storage performance.

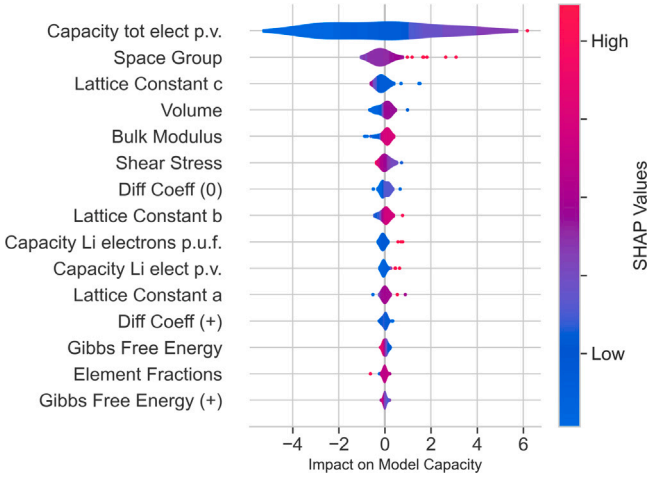

Fig. 6. SHAP summary plot illustrating the impact of structural properties on the functional performance of battery anode materials. Each dot represents a feature's influence on the model's output, with the horizontal position indicating the magnitude and direction of the impact (positive or negative). The colour of the dots represents the feature's value (blue for low, red for high). For example, a red dot far to the right for feature 'X' indicates a high value of 'X' strongly increases performance (target property values), while a blue dot far to the left for feature 'Y' indicates a low value of 'Y' strongly decreases performance (target property values). This plot highlights how different values of each feature affect the model's predictions and their relative importance. (For interpretation of the references to colour in this figure legend, the reader is referred to the web version of this article.)

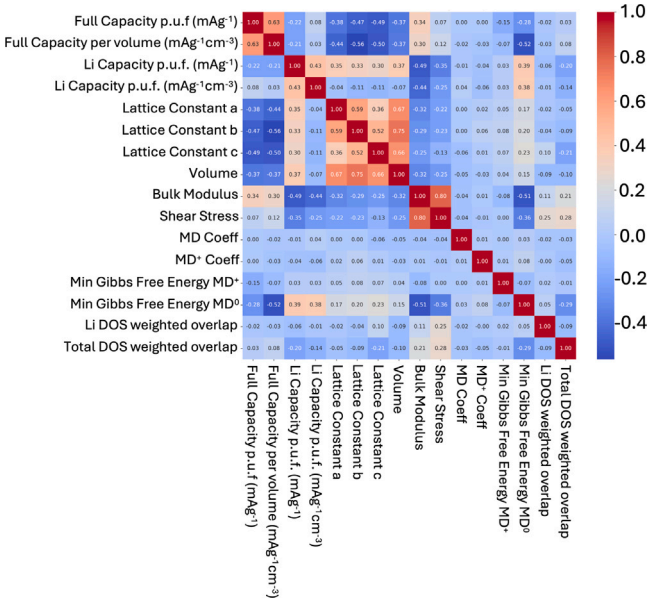

Fig. 7. Correlation Matrix of the calculated properties. This includes total electronic capacity per formula unit in milliampere per gram (mAg^{-1}), volume occupied by the total electronic capacity, capacity due to lithium electrons per formula unit (mA^{-1}), capacity of lithium electrons per unit volume ($mA^{-1}cm^{-3}$), and others. "Lattice Constant a", "b", and "c" represent the lattice parameters and "Volume" refers to the unit cell volume. "Bulk Modulus" and "Shear Stress" measure material resistance to uniform compression and shear deformation, respectively. "MD Coeff" and "MD+ Coeff" represent coefficients from molecular dynamics simulations, with "MD+" indicating enhanced sampling techniques. "Min Gibbs Free Energy (eV) MD" and "MD+" show the minimum Gibbs free energy from standard and enhanced molecular dynamics simulations, respectively. "Li DOS weighted overlap" and "total DOS weighted overlap" describe the weighted overlap integrals for lithium interstitial sites and the total system, providing insights into diffusion pathways. The *x*-axis reports the same properties ordered from left to right so the correlation will be 1 along the diagonal.

Multivariable correlations

Initially, a conventional statistical analysis revealed no clear correlation between density overlap and ion diffusion rates. This indicates that simple metrics derived from partial density of states (pDOS) calculations alone are not sufficient to predict overall anode electrochemical performance. In other words, relying solely on basic pDOS-based descriptors does not yield meaningful insights into how easily ions might move through the material.

To gain deeper understanding, we employed a range of ML-driven, high-dimensional data analyses. These techniques allowed us to move beyond simple pairwise correlations and to consider multiple material properties and descriptors simultaneously. By examining the combined influence of elemental composition and crystal symmetry on mechanical, electronic, and ionic transport properties, our ML models revealed more complex relationships than those accessible through basic statistical tests. Specifically, while elemental composition influences chemical bonding and electrochemical behaviour, the symmetry of the crystal structure plays a key role in governing ionic diffusivity and mechanical stability (see Figs. 4 and 5). These results highlight that a material's underlying symmetry can shape how lithium ions move through its lattice and how well it resists deformation during operation.

Further correlation analyses, illustrated in Fig. 7, identified a significant negative correlation between bulk modulus and shear stress on one hand, and Gibbs free energy under Li^0 conditions on the other. This suggests that materials with higher bulk moduli may more effectively withstand the mechanical strains caused by lithium intercalation, maintaining their structural integrity. Moreover, the relationship between shear stress and lithium orbital overlap points to lithium's critical role in influencing the material's micro-hardness. Here again, the ML-driven correlation analysis goes beyond simple observations, linking mechanical strength directly to how lithium is incorporated into the lattice.

To dissect the contribution of individual features to the ML model predictions, we employed SHapley Additive exPlanations (SHAP) analysis. SHAP offers a game-theoretic approach to interpret ML outputs, allowing us to pinpoint which structural and electronic properties are most influential in determining functional behaviour. As shown in Fig. 6, features are ranked by their importance, providing a clear visualisation of how various factors – ranging from atomic composition and crystal symmetry to electronic descriptors – interact to shape material performance.

In addition to multivariable correlation analysis, SHAP analysis (Fig. 6) reveals that structural and mechanical descriptors, such as space group, lattice constants, and bulk modulus, have a greater impact on the model's capacity predictions than elemental fractions or individual electronic descriptors. This finding emphasises that compositional trends alone are insufficient to reliably predict high performance, and that the crystal symmetry and mechanical robustness must be considered as primary factors. Moreover, the correlation analysis (Fig. 7) highlights that full capacity tends to decrease with increasing volume, Gibbs free energy, and density of states (DOS) overlap, suggesting a delicate trade-off between electronic conductivity and lithium storage capability. Overall, these results underscore the critical need for holistic, multi-parameter screening strategies when identifying and designing next-generation anode materials.

Interestingly, while we do observe a correlation between crystal space group and micro-hardness, this influence appears more moderate than previously found in studies limited to Si-C anodes [68]. In the more diverse dataset analysed here, the crystal symmetry effect is diluted by the greater complexity introduced by multiple elements and structural variations, illustrating how ML methods can reveal subtle dependencies that differ from simpler, more constrained systems.

Finally, our ML models also shed light on the role of electronic overlap in energy storage. The negative correlation with capacity suggests a trade-off: although higher electronic overlap might enhance conductivity, it could simultaneously lower the material's ability to store lithium ions effectively. Such detailed insights, uncovered through ML-driven

analyses, underscore the importance of balancing electronic, structural, and mechanical properties to optimise overall battery performance.

While the multivariable analysis presented here reveals important correlations between elemental composition, crystal symmetry, and anode material performance, it is important to acknowledge the inherent limitations of this approach. The trends identified are based on a finite dataset of structures and chemistries, and may not capture the full diversity of possible anode candidates, especially those involving different anionic species or non-oxide materials. Moreover, the complex interplay between electronic, structural, and mechanical properties suggests that no single elemental "fingerprint" universally guarantees high performance. Instead, these findings highlight the necessity of integrating broad compositional diversity and careful structural characterisation when developing general design principles for next-generation anode materials.

4. Conclusion

In this study, we employed advanced computational methods to identify and evaluate promising candidates for alternative lithium-ion battery anode materials. By systematically exploring stable, thermodynamically favourable crystal structures composed of Li, Si, C, O, N, B, F, Fe, Ni, Co, and Mn, we analysed how their electronic, structural, thermodynamic, and mechanical properties influence lithium storage capacity. This comprehensive analysis identified several new materials exhibiting favourable characteristics comparable to, or exceeding, conventional anodes.

Among the best-performing candidates are $Li_{47}Ni_8O_{32}$, $Li_{35}Fe_8O_{32}$, $Li_{84}Si_{20}$, $Li_{56}Mn_8N_{32}$, $Li_{16}Si_2O_{12}$, and $Li_{24}Co_4O_{16}$. $Li_{84}Si_{20}$ stands out for its high Maximum Theoretical Capacity (MTC), surpassing that of pure silicon, and its favourable Gibbs free energy, making it an excellent candidate for high-capacity, long-lasting battery anodes. $Li_{56}Mn_8N_{32}$, enriched with nitrogen and manganese, offers a suitable electrochemical profile combined with robust mechanical properties, which should enhance structural stability and potentially improve the battery's lifespan. Meanwhile, $Li_{16}Si_2O_{12}$ density of states shows a pronounced overlap, suggesting efficient lithium accommodation and suggesting its potential for high-capacity storage. $Li_{24}Co_4O_{16}$, on the other hand, demonstrates notable electronic conductivity and favourable lithium-ion mobility, indicating potential rapid charge–discharge cycles and high rate capability desirable in high-power applications.

While our integrated DFT and ML approach enables efficient and scalable screening of a large number of candidate structures, several limitations must be acknowledged. The accuracy of the ML models is inherently dependent on the quality and diversity of the DFT training data; biases or under-represented chemistries in the training set could affect model generalisability. Ensemble models such as Random Forest and XGBoost, despite their strength in handling non-linearity, remain somewhat opaque in terms of interpretability. and although SHAP values provide local explanations, they do not uncover causal mechanisms and may sometimes conflict across features. Finally, our study focuses on theoretical performance metrics; experimental validation of top candidates is necessary to confirm their viability as commercial anodes. Furthermore, although our analysis identified important trends linking elemental composition to performance, the diversity of structural environments and property interdependencies indicates that no single elemental combination universally ensures optimal anode behaviour. The complex interplay between composition, symmetry, and electronic structure underscores the necessity of a holistic, multi-parameter screening approach for future anode design.

Despite these limitations, our methodology – integrating DFT, machine learning, and interpretability tools – provides a scalable framework for investigating large chemical spaces. This approach assists both fundamental research and industrial R&D by rapidly identifying structures with ideal theoretical performance. The exploration of materials derived from photovoltaic waste elements opens pathways to more sustainable energy storage technologies. The insights gained here, including the emphasis on thermodynamic stability, ion mobility, mechanical hardness, and electronic structure, contribute to developing next-generation lithium-ion battery anodes that balance high performance with environmental and economic considerations. By analysing these key material attributes, this work charts a direction towards practical, stable, and efficient battery anodes suitable for future energy storage solutions.

CRediT authorship contribution statement

Marco Fronzi: Writing – review & editing, Writing – original draft, Methodology, Investigation, Formal analysis, Data curation, Conceptualization. **Catherine Stampfl:** Writing – review & editing. **Amanda Ellis:** Project administration, Conceptualization. **Eirini Goudeli:** Writing – review & editing, Supervision.

Declaration of competing interest

The authors declare that they have no known competing financial interests or personal relationships that could have appeared to influence the work reported in this paper.

Acknowledgements

The authors would like to acknowledge the Future Batteries Industries CRC and project participants for funding the Super Anode Project, and the ARC FL230100176. The theoretical calculations in this research were undertaken with the assistance of resources from the National Computational Infrastructure (NCI), which is supported by the Australian Government.

Appendix A. Supplementary data

Supplementary material related to this article can be found online at https://doi.org/10.1016/j.jpowsour.2025.237347.

Data availability

Data will be made available on request.

References

[1] J. Khan, M.H. Arsalan, Solar power technologies for sustainable electricity generation–A review, Renew. Sustain. Energy Rev. 55 (2016) 414–425.
[2] G.N. Newton, L.R. Johnson, D.A. Walsh, B.J. Hwang, H. Han, Sustainability of battery technologies: today and tomorrow, ACS Sustain. Chem. Eng. 9 (19) (2021) 6507–6509.
[3] M. Tao, V. Fthenakis, B. Ebin, B.-M. Steenari, E. Butler, P. Sinha, R. Corkish, K. Wambach, E.S. Simon, Major challenges and opportunities in silicon solar module recycling, Prog. Photovolt., Res. Appl. 28 (10) (2020) 1077–1088.
[4] P.R. Dias, L. Schmidt, N.L. Chang, M.M. Lunardi, R. Deng, B. Trigger, L.B. Gomes, R. Egan, H. Veit, High yield, low cost, environmentally friendly process to recycle silicon solar panels: Technical, economic and environmental feasibility assessment, Renew. Sustain. Energy Rev. 169 (2022) 112900.
[5] M.S. Chowdhury, K.S. Rahman, T. Chowdhury, N. Nuthammachot, K. Techato, M. Akhtaruzzaman, S.K. Tiong, K. Sopian, N. Amin, An overview of solar photovoltaic panels' end-of-life material recycling, Energy Strat. Rev. 27 (2020) 100431.
[6] Y. Xu, J. Li, Q. Tan, A.L. Peters, C. Yang, Global status of recycling waste solar panels: A review, Waste Manage. 75 (2018) 450–458.
[7] Q. Liao, S. Li, F. Xi, Z. Tong, X. Chen, X. Wan, W. Ma, R. Deng, High-performance silicon carbon anodes based on value-added recycling strategy of end-of-life photovoltaic modules, Energy 281 (2023) 128345, http://dx.doi.org/10.1016/j.energy.2023.128345, URL https://www.sciencedirect.com/science/article/pii/S0360544223017395.
[8] L. Zhang, Z. Xu, Towards minimization of secondary wastes: Element recycling to achieve future complete resource recycling of electronic wastes, Waste Manage. 96 (2019) 175–180.

[9] T. Georgi-Maschler, B. Friedrich, R. Weyhe, H. Heegn, M. Rutz, Development of a recycling process for li-ion batteries, J. Power Sources 207 (2012) 173–182.

[10] I. Sultana, Y. Chen, S. Huang, M.M. Rahman, Recycled value-added circular energy materials for new battery application: Recycling strategies, challenges, and sustainability-a comprehensive review, J. Environ. Chem. Eng. (2022) 108728.

[11] G.A. Heath, T.J. Silverman, M. Kempe, M. Deceglie, D. Ravikumar, T. Remo, H. Cui, P. Sinha, C. Libby, S. Shaw, et al., Research and development priorities for silicon photovoltaic module recycling to support a circular economy, Nat. Energy 5 (7) (2020) 502–510.

[12] H.-J. Kim, T. Krishna, K. Zeb, V. Rajangam, C.V.M. Gopi, S. Sambasivam, K.V.G. Raghavendra, I.M. Obaidat, A comprehensive review of li-ion battery materials and their recycling techniques, Electronics 9 (7) (2020) 1161.

[13] H. Groult, D. Devilliers, M. Vogler, P. Marcus, F. Nicolas, Effect of chemical fluorination of carbon anodes on their electrochemical properties in KF-2HF, J. Electrochem. Soc. 144 (10) (1997) 3361.

[14] M.I. Eremets, A.G. Gavriliuk, I.A. Trojan, D.A. Dzivenko, R. Boehler, Single-bonded cubic form of nitrogen, Nat. Mater. 3 (8) (2004) 558–563.

[15] D. Sakamaki, S. Ghosh, S. Seki, Dynamic covalent bonds: approaches from stable radical species, Mater. Chem. Front. 3 (11) (2019) 2270–2282.

[16] C. Liu, S. Yuan, Y. Yang, X.-X. Zhao, X. Duan, B. Cao, Q. Wang, Prussian blue analogues-derived nitrogen-doped carbon-coated FeO/CoO hollow nanocages as a high-performance anode material for Li storage, Rare Met. 42 (12) (2023) 4070–4080.

[17] R. Yi, J. Zai, F. Dai, M.L. Gordin, D. Wang, Improved rate capability of Si–C composite anodes by boron doping for lithium-ion batteries, Electrochem. Commun. 36 (2013) 29–32.

[18] J. Zhao, L. Liao, F. Shi, T. Lei, G. Chen, A. Pei, J. Sun, K. Yan, G. Zhou, J. Xie, et al., Surface fluorination of reactive battery anode materials for enhanced stability, J. Am. Chem. Soc. 139 (33) (2017) 11550–11558.

[19] H.W. Hugosson, U. Jansson, B. Johansson, O. Eriksson, Phase stability diagrams of transition metal carbides, a theoretical study, Chem. Phys. Lett. 333 (6) (2001) 444–450.

[20] B. Xu, M. Zheng, H. Tang, Z. Chen, Y. Chi, L. Wang, L. Zhang, Y. Chen, H. Pang, Iron oxide-based nanomaterials for supercapacitors, Nanotechnology 30 (20) (2019) 204002.

[21] R. Xia, K. Zhao, L.-Y. Kuo, L. Zhang, D.M. Cunha, Y. Wang, S. Huang, J. Zheng, B. Boukamp, P. Kaghazchi, et al., Nickel niobate anodes for high rate lithium-ion batteries, Adv. Energy Mater. 12 (1) (2022) 2102972.

[22] G. Wang, Y. Chen, K. Konstantinov, J. Yao, J.-h. Ahn, H. Liu, S. Dou, Nanosize cobalt oxides as anode materials for lithium-ion batteries, J. Alloys Compd. 340 (1–2) (2002) L5–L10.

[23] Y. Deng, L. Wan, Y. Xie, X. Qin, G. Chen, Recent advances in mn-based oxides as anode materials for lithium ion batteries, Rsc Adv. 4 (45) (2014) 23914–23935.

[24] P.-H. Chen, W.-S. Chen, C.-H. Lee, J.-Y. Wu, Comprehensive review of crystalline silicon solar panel recycling: From historical context to advanced techniques, Sustainability 16 (1) (2023) 60.

[25] M.A. Franco, S.N. Groesser, A systematic literature review of the solar photovoltaic value chain for a circular economy, Sustainability 13 (17) (2021) 9615.

[26] F. Yamashita, Y. Ide, H. Akamine, K. Ishikawa, M. Nishida, Effect of C/O ratio on phase change and stability of inclusions in Ti–Ni alloys fabricated by a commercial production process, Shape Mem. Superelasticity 6 (2020) 354–364.

[27] J. Kuang, Z. Li, W. Li, C. Chen, M. La, Y. Hao, Achieving high activity and long-term stability towards oxygen evolution in acid by phase coupling between CeO2-Ir, Materials 16 (21) (2023) 7000.

[28] H.Y. Kim, S. Miyazaki, et al., Effects of oxygen concentration and phase stability on nano-domain structure and thermal expansion behavior of Ti–Nb–Zr–Ta–O alloys, Acta Mater. 100 (2015) 313–322.

[29] M. Fronzi, R.D. Amos, et al., Evaluation of machine learning interatomic potentials for the properties of gold nanoparticles, Nanomaterials 12 (21) (2022) 3891.

[30] M. Fronzi, et al., Active learning in Bayesian neural networks for the bandgap predictions of novel Van der Waals heterostructures, Adv. Intell. Syst. (2100080) (2021) 1–7.

[31] G. Kresse, J. Hafner, Ab initio molecular dynamics for liquid metals, Phys. Rev. B 47 (1993) 558.

[32] G. Kresse, J. Furthmüller, Efficiency of ab-initio total energy calculations for metals and semiconductors using a plane-wave basis set, Comput. Mater. Sci. 6 (1996) 15.

[33] G. Kresse, J. Furthmüller, Efficient iterative schemes for ab initio total-energy calculations using a plane-wave basis set, Phys. Rev. B 54 (1996) 11169.

[34] G. Kresse, J. Hafner, Norm-conserving and ultrasoft pseudopotentials for first-row and transition elements, J. Phys.: Condens. Matter. 6 (1994) 8245.

[35] G. Kresse, D. Joubert, From ultrasoft pseudopotentials to the projector augmented-wave method, Phys. Rev. 59 (1999) 1758.

[36] J.P. Perdew, K. Burke, M. Ernzerhof, Generalized gradient approximation made simple, Phys. Rev. Lett. 77 (18) (1996) 3865–3868.

[37] S. Nosé, A molecular dynamics method for simulations in the canonical ensemble, Mol. Phys. 52 (2) (1984) 255–268.

[38] S.L. Seyler, C.E. Seyler, Molecular hydrodynamic theory of the velocity autocorrelation function, J. Chem. Phys. 159 (5) (2023).

[39] L. Ward, A. Agrawal, A. Choudhary, C. Wolverton, A general-purpose machine learning framework for predicting properties of inorganic materials, Npj Comput. Mater. 2 (1) (2016) 1–7.

[40] Y. Luo, H. Chen, J. Wang, X. Niu, Machine-learning-assisted discovery of boron-doped graphene with high work function as an anode material for Li/Na/K-ion batteries, Phys. Chem. Chem. Phys. 25 (17) (2023) 12200–12206.

[41] C. Chowdhury, P. Gain, A. Datta, Evolutionary structure prediction-assisted design of anode materials for Ca-ion battery based on phosphorene, Phys. Chem. Chem. Phys. 23 (15) (2021) 9466–9475.

[42] M. Imani, A. Beikmohammadi, H.R. Arabnia, Comprehensive analysis of random forest and xgboost performance with SMOTE, ADASYN, and GNUS under varying imbalance levels, Technologies 13 (3) (2025) 88.

[43] H. Qin, Y. Zhang, Z. Guo, S. Wang, D. Zhao, Y. Xue, Prediction of bandgap in lithium-ion battery materials based on explainable boosting machine learning techniques, Materials 17 (24) (2024) 6217.

[44] M. Faraji Niri, K. Aslansefat, S. Haghi, M. Hashemian, R. Daub, J. Marco, A review of the applications of explainable machine learning for lithium–Ion batteries: From production to state and performance estimation, Energies 16 (17) (2023) 6360, http://dx.doi.org/10.3390/en16176360.

[45] X. Shi, L. Zhou, Y. Huang, Y. Wu, Z. Hong, Machine learning assisted screening of metal binary alloys for anode materials, 2024, arXiv preprint arXiv:2409.09583.

[46] Y. Kim, Y. Kim, Explainable heat-related mortality with random forest and shapley additive explanations (SHAP) models, Sustain. Cities Soc. 79 (2022) 103677.

[47] G. Van den Broeck, A. Lykov, M. Schleich, D. Suciu, On the tractability of SHAP explanations, J. Artificial Intelligence Res. 74 (2022) 851–886.

[48] A. Eftekhari, On the Theoretical Capacity/energy of Lithium Batteries and Their Counterparts, ACS Publications, 2018.

[49] B. Liang, Y. Liu, Y. Xu, Silicon-based materials as high capacity anodes for next generation lithium ion batteries, J. Power Sources 267 (2014) 469–490.

[50] R. Moshtev, P. Zlatilova, B. Puresheva, V. Manev, Material balance of petroleum coke/LiNiO2 lithium-ion cells, J. Power Sources 56 (2) (1995) 137–144.

[51] R. Taylor, P.A. Wood, A million crystal structures: The whole is greater than the sum of its parts, Chem. Rev. 119 (16) (2019) 9427–9477.

[52] T.P. Nguyen, T.T. Giang, I.T. Kim, Restructuring NiO to LiNiO2: Ultrastable and reversible anodes for lithium-ion batteries, Chem. Eng. J. 437 (2022) 135292.

[53] Y. Ma, J.H. Teo, D. Kitsche, T. Diemant, F. Strauss, Y. Ma, D. Goonetilleke, J. Janek, M. Bianchini, T. Brezesinski, Cycling performance and limitations of LiNiO2 in solid-state batteries, ACS Energy Lett. 6 (9) (2021) 3020–3028.

[54] M. Iftikhar, S. Latif, V. Jevtovic, I. Ashraf, A.A. El-Zahhar, E.A.M. Saleh, S.M. Abbas, et al., Current advances and prospects in nio-based lithium-ion battery anodes, Sustain. Energy Technol. Assess. 53 (2022) 102376.

[55] A.G. Hailemariam, Z. Syum, T.T. Mamo, M. Qorbani, C.-R. Hsing, A. Sabbah, S. Quadir, K.S. Bayikadi, H.-L. Wu, C.-M. Wei, et al., Oxygen-incorporated lithium-rich iron sulfide cathodes for Li-ion batteries with boosted material stability and electrochemical performance, Chem. Mater. 36 (19) (2024) 9370–9379.

[56] C. Cai, D. Zhang, Q. Zhang, K. Chen, W. Hua, C. Peng, D. Xue, Origin of oxygen-redox and transition metals dissolution in Ni-rich LixNi0. 8Co0. 1Mn0. 1O2 cathode, J. Chem. Phys. 158 (11) (2023).

[57] S.-P. Guo, Z. Ma, J.-C. Li, H.-G. Xue, First investigation of the electrochemical performance of γ-LiFeO 2 micro-cubes as promising anode material for lithium-ion batteries, J. Mater. Sci. 52 (2017) 1469–1476.

[58] Y. Hu, α-LiFe5O8: A promising iron-based anode material for lithium-ion batteries, Mater. Sci. Eng.: B 297 (2023) 116792.

[59] R.A. Bajwa, U. Farooq, S. Ullah, M. Salman, S. Haider, R. Hussain, Metal-organic framework (MOF) attached and their derived metal oxides (Co, Cu, Zn and Fe) as anode for lithium ion battery: A review, J. Energy Storage 72 (2023) 108708.

[60] X. Li, C. Wang, Engineering nanostructured anodes via electrostatic spray deposition for high performance lithium ion battery application, J. Mater. Chem. A 1 (2) (2013) 165–182.

[61] A. Eftekhari, Low voltage anode materials for lithium-ion batteries, Energy Storage Mater. 7 (2017) 157–180.

[62] C.-C. Hsieh, W.-R. Liu, Effects of nitrogen doping on Si/carbon composite anode derived from Si wastes as potential active materials for Li ion batteries, J. Alloys Compd. 790 (2019) 829–836.

[63] Y. Ma, A. Huang, Y. Li, H. Jiang, W. Zhang, L. Zhang, L. Li, S. Peng, Simple preparation of Si/N-doped carbon anodes from photovoltaic industry waste for lithium-ion batteries, J. Alloys Compd. 890 (2022) 161792.

[64] Y. Zhou, E. Roginskii, K.V. Smirnov, M.B. Smirnov, A.S. Savin, O. Nguyen, J.-P. Pereira-Ramos, R. Baddour-Hadjean, Insights into the electronic structure and vibrational dynamics of Li_7MnN_4 anode material for Li-ion batteries: A combined experimental and computational study, J. Alloys Compd. 934 (2023) 167987, http://dx.doi.org/10.1016/j.jallcom.2023.167987.

[65] N. Emery, É. Panabière, N. Brétéché, K. Djellab, E. Janod, L. Cario, M. Saubanere, M. Gabás, J.-M. Tarascon, C. Masquelier, M. Courty, Unidimensional unit cell variation and Fe^{3+}/Fe^{4+} redox activity of Li_3FeN_2 in Li-ion batteries, J. Alloys Compd. 722 (2017) 157–167, http://dx.doi.org/10.1016/j.jallcom.2017.06.337.

[66] C. Ben Mahmoud, A. Anelli, G. Csányi, M. Ceriotti, Learning the electronic density of states in condensed matter, Phys. Rev. B 102 (23) (2020) 235130.

[67] P. Anderson, Y. Liu, DFT analysis of $LiCoO_2$ and its derivatives, Electrochim. Acta 330 (2020) 135–142.
[68] M. Fronzi, A. Ellis, E. Goudeli, Silicon-based anodes for Li batteries: Thermodynamics, structural analysis, and Li diffusion, J. Phys. Chem. Lett. 14 (2023) 10388–10395.
[69] Q.-K. Wang, C.-C. Chai, Q.-Y. Fan, Y.-T. Yang, Physical properties of C-Si alloys in C2/m structure, Commun. Theor. Phys. (Beijing) 68 (2) (2017) 259.
[70] R. Yu, X. Chong, Y. Jiang, R. Zhou, W. Yuan, J. Feng, The stability, electronic structure, elastic and metallic properties of manganese nitrides, RSC Adv. 5 (2) (2015) 1323–1330, http://dx.doi.org/10.1039/C4RA10914G.
[71] H. Osgood, S.V. Devaguptapu, H. Xu, J. Cho, G. Wu, Transition metal (Fe, Co, Ni, and Mn) oxides for oxygen reduction and evolution bifunctional catalysts in alkaline media, Nano Today 11 (5) (2016) 601–625.